



A comparative study on mesocellular foam silica with different template removal methods and their effects on enzyme immobilization

Nithi Thananukul¹ · Angkana Phongphut¹ · Seeroong Prichanont¹ · Chanchana Thanachayanont² · Sarah Fearn³ · Bralee Chayasombat²

Published online: 6 December 2018
© Springer Science+Business Media, LLC, part of Springer Nature 2018

Abstract

Mesocellular foam silica (MCF) was synthesized using Pluronic P-123 triblock copolymer as a template. Calcination and solvent extraction were employed to remove templates and compared. Through physical, chemical and functional characterization interesting results have been observed. Microstructures of the two MCFs were very different. Pore structure of the calcined MCF was found to be more ordered than that of the solvent extracted MCF. However, pores of the solvent extracted MCF seemed more defined and spongy under SEM observations. Surface functional groups and their concentrations characterized by ToF-SIMS were also found to be different. Surface silanol groups were found to be more concentrated in the calcined MCF. Each type of MCFs was subsequently grafted by an amine functional group, adsorbed by Au ion precursors, and reduced to form Au nanoparticles (AuNPs) on the MCF surfaces. These decorated MCF surfaces were immobilized with enzyme acetylcholinesterase (AChE), modified on screen-printed carbon electrodes and tested for electrochemical responses with acetylthiocholine. AuNPs were successfully distributed within the pores for both types of MCFs. Before the functional biosensor electrochemical tests, calcination seemed more promising than solvent extraction due to periodic structure of pores, high surface area, less contamination and higher concentration of surface silanol groups available for grafting of the amine functional group. However, after immobilization of the AuNPs for electron transport improvement and enzyme immobilization, a few observations of biosensing performances were noteworthy. Firstly, having AuNPs distributed throughout the MCF structure did not help the electron transport. Results of reduced response currents from both types of MCFs compared to MCFs without AuNPs indicated that MCF walls were too thick to allow electron transport. Secondly, the higher concentration of surface silanol groups in calcined MCFs resulted in Ostwald's ripening of small AuNPs giving bigger AuNPs than the case of solvent extraction. Therefore, although the AuNPs in enzyme biosensors are expected to help electron transport and enzyme immobilization, this study showed that although the former did not occur, the latter was well demonstrated. The smaller AuNPs in the solvent extraction case resulted in higher surface area than the bigger AuNPs in the calcination case. This was the reason why the response current was higher for the solvent extracted MCFs compared to the calcined MCFs.

Keywords Mesocellular foam silica · Template removal · Microstructure · Surface chemistry · Enzyme support

Electronic supplementary material The online version of this article (<https://doi.org/10.1007/s10934-018-0705-1>) contains supplementary material, which is available to authorized users.

✉ Bralee Chayasombat
braleec@mtec.or.th

¹ Department of Chemical Engineering, Faculty of Engineering, Chulalongkorn University, Phayathai Road, Bangkok 10330, Thailand

² National Metal and Materials Technology Center, Thailand Science Park, Paholyothin Road, Pathumthani 12120, Thailand

³ Department of Materials, Faculty of Engineering, Imperial College, London SW7 2AZ, UK

1 Introduction

Mesoporous silicas (MPSs) are unique and can be tailored to desirable pore structures for versatile applications. With internal pore sizes in a range of 2–50 nm, pore structure of the MPSs depends on the formulations and methods of synthesis [1, 2]. Thus, various MPSs such as channel-like (SBA-15 and MCM-41), cubic-like (SBA-16), and bottle-neck-like (mesocellular foam silica; MCF) can be achieved. Not only can MPSs be easily tuned for specific pore structures and sizes, but they can also be surface modified via abundant silanol groups. As a result, custom-fit MPSs are available for specific applications, such as an adsorbent for environmental toxic gases, energy production and storage, catalysis and sensors [3–9]. Among all possible forms of MPSs, MCF composing of uniform spherical cells interconnected by windows [10], gives a 3D pore network resulting in a better substance diffusion than a 2D pore structure of conventional MPSs such as SBA-15 or MCM-41 [11]. Moreover, the pore and window sizes of MCF are readily tunable by adjusting surfactant (template), swelling agent and silica source ratio [12]. These advantages make MCF suitable for applications that require pore size tuning such as supports for enzyme immobilization. Immobilization of enzymes on MCF is affected directly by the surface chemistry of the MCF. Furthermore, noble metal nanoparticles, such as Au, decorated on the surfaces of MPSs have been reported to help promoting electron transfer as well as enhancing enzyme loading, stability and activity [13, 14]. However, this process depends strongly on the surface chemistry of the MPSs.

One of the factors affecting surface chemistry of the MCF is the template removal method [8, 9]. Calcination at high temperature (500–600 °C) is currently most widely applied. This method can completely remove organic templates, but some studies have reported pore contraction during calcination [15–17]. Alternatively, the solvent extraction method is a more environmental friendly process and a re-use of the organic template is also possible which benefits a mass production of mesoporous materials [18]. Many studies have reported incomplete template removal and a reduction in crystallinity of the obtained materials by utilizing the solvent extraction method [19–21]. To obtain desirable final structure and the surface chemistry, in-depth characterization of nanostructure and matching functional properties to applications from each template removal method are required.

In this study, spherical MCF was synthesized by a modified method [22]. Then, two template removal methods were applied, i.e., calcination and extraction by ethanol solvent. After template removal, both types of MCFs were functionalized with an amine functional group.

Functionalized MCFs were adsorbed by Au precursors at different adsorption times and concentrations, before being chemically reduced by NaBH₄ to form Au nanoparticle/MCF composites. The MCFs before and after functionalization and Au decoration were comparatively characterized using multiple techniques, such as thermal gravitation analysis (TGA), Fourier transform infrared spectroscopy (FTIR), time-of-flight secondary ion mass spectroscopy (ToF-SIMS), X-ray diffraction (XRD), scanning electron microscopy (SEM) and transmission electron microscopy (TEM). MCFs with and without gold decoration with different Au precursor concentrations were immobilized with the enzyme AChE, modified on the screen-printed carbon electrodes and tested for their response to acetylthiocholine by studying electrochemical characteristics. This study aims to identify different physical and chemical properties of the MCFs prepared using different template removal methods, and how the differences affect their performances as support materials for enzyme immobilization.

2 Materials and methods

2.1 Syntheses

All chemicals were of analytical grade and used without further purification. 2 g of Pluronic P-123 triblock copolymer (BASF, USA), a structure directing agent, was dissolved in 1.6 M HCl solution. After mixing, 3.4 ml of 1,3,5-trimethylbenzene (TMB; Sigma–Aldrich) was added to the solution and heated to 40 °C for 2 h under vigorous stirring. Then 9.2 ml of the silica source, tetraethoxysilane (TEOS; 98% purity, Sigma–Aldrich), was added and mixed. The mixture was subsequently aged in a Teflon bottle at 40 °C for 20 h under static condition and at 100 °C for another 20 h. The obtained particles were consecutively washed with ethanol and deionized water until the pH of the filtrate was not changed, and dried for 24 h at ambient temperature. Next, the template removal was carried out by (a) calcination at 550 °C for 6 h under air flow or (b) extraction by ethanol solvent. The ethanol extraction was done by refluxing 1.5 g MCF with a mixture of 100 ml ethanol and 1 ml concentrated HCl for 24 h at 90 °C using a soxhlet extractor. The MCFs achieved from both methods were then functionalized with 3-Aminopropyl triethoxysilane (APTES; Fluka) to modify the surface charge of the MCFs [23]. The functionalized MCFs were then decorated with gold nanoparticles by adsorption of Au precursors ((HAuCl₄·3H₂O) 98% purity; Sigma–Aldrich) with concentrations from 0.1 to 10.0 mM for 1–6 h. The adsorbed gold precursors were finally reduced by 0.1 M NaBH₄ (Sigma–Aldrich) aqueous solution for 10 min. The products were washed with DI water and air dried.

2.2 Characterization

Both the calcined MCF and the solvent extracted MCF before and after functionalization and decoration of gold nanoparticles were systematically characterized using Thermogravimetric analysis (TGA; Mettler Toledo, TGA/SDTA 851), Fourier transformed infrared (FTIR; Perkin Elmer 1760x), N_2 adsorption–desorption isotherms (Quantachrome autosorb-1), X-ray diffraction (XRD; Rigaku TTRAX III), field emission scanning electron microscopy (FE-SEM; JEOL JSM-5410) and transmission electron microscopy (TEM; JEOL JEM-2010). The pore and window size analyses were conducted from the adsorption–desorption isotherms using BdB-FHH model [24]. Furthermore, the surface chemistry of the calcined MCF and the extracted MCF were studied using the time-of-flight secondary ions mass spectroscopy (ToF-SIMS).

2.3 Electrochemical testing

The immobilization of AChE within MCF/APTES/AuNPs was initiated by dissolving 0.001 g AChE in 2 ml PBS 0.1 M pH 6 under mild stirring at 4 °C. Then, MCF/APTES/AuNPs was added to homogenize the prepared solution with mild continuous stirring at 4 °C for 2 h. The particles were then filtered and washed with 0.1 M PBS (pH 6) to remove unattached enzymes. For the electrode modification, 0.05 g of MCFs were added to 1 ml of 0.1 M PBS solution (pH 6)

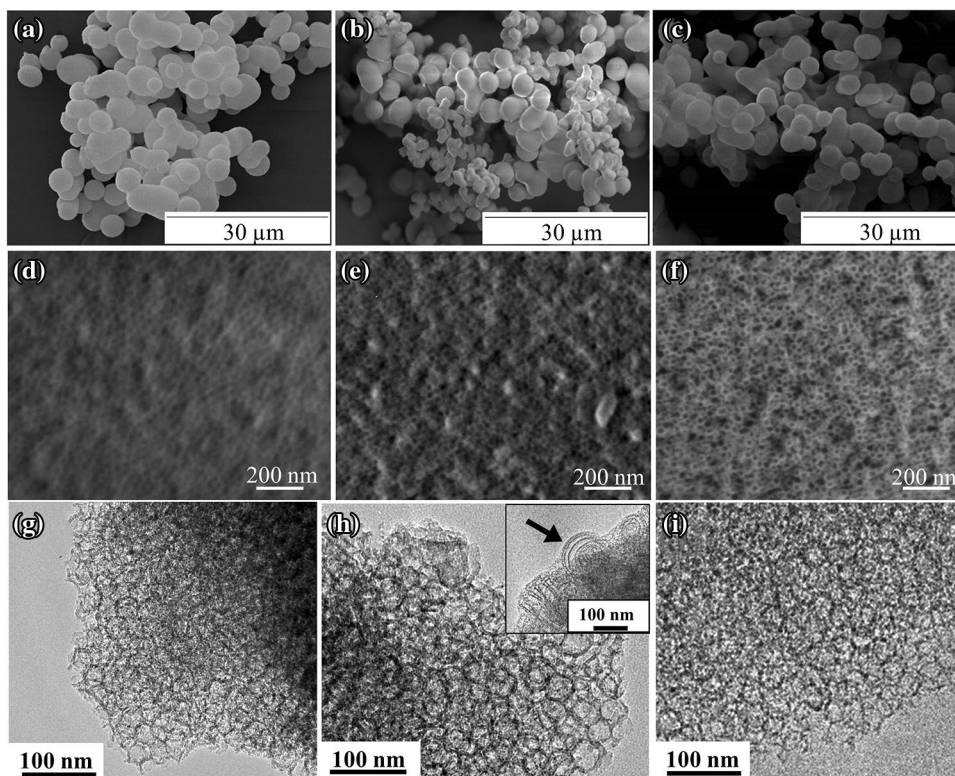
and stirred to homogeneity. Then 3 μ l of the mixture was dropped on a screen printed carbon electrode (SPCE). After drying at room temperature for 20 min, 3 μ l of chitosan solution (0.05% w/v in 1% v/v acetic acid solution) was dropped over the MCF/SPCE to fix the MCFs onto the electrode, and dried in a desiccator before use. The modified SPCEs were tested by cyclic voltammetry (CV) measurements for pesticide detection by measuring the electrochemical reaction with 10 mM of acetylthiocholine in pH 9.0 phosphate buffer solution. The apparatus used was an Autolab potentiostat (Metrohm PGSTAT101) consisting respectively of the modified electrode as a working, a Pt wire as a counter and a Ag/AgCl reference electrode.

3 Results and discussion

3.1 Characterization of MCFs

Figure 1a–c show low magnification, and Fig. 1d–f high magnification SEM images of as-synthesized MCF, calcined MCF and solvent extracted MCF particles, respectively. An average particle size of the as-synthesized MCF is 3.5 μ m ($n = 200$), while the size reduces to 2.0 μ m ($n = 200$) and 3.0 μ m ($n = 200$), respectively, for the calcined and solvent extracted MCF. The particle size reduction of the calcined MCF resulted from solid-state sintering process where atomic diffusion in the solid produces joining of particles

Fig. 1 Low and high magnification SEM images of the **a, d** as-synthesized, **b, e** calcined and **c, f** solvent extracted MCFs. **g–i** shows TEM images of as-synthesized, calcined and solvent extracted MCFs, respectively



and reduction of porosity. Notably non uniform particle size distribution is observed for the case of the calcined MCF which may be caused by random densification, restructuring and collapsing of the porous structure. On the contrary, the deformation is not observed in the case of the solvent extracted MCF, Fig. 1c. Figure 1d shows the surface of an as-synthesized MCF particle. The pores are mostly closed. The presence of organics from the synthesis process made it difficult to focus the image at such a high magnification. Figure 1e, f show surfaces of the calcined and solvent extracted MCFs where open pore structures are clearly observed. The pore sizes of the solvent extracted MCF are slightly bigger than those of the calcined MCF, i.e., approximately 15.2 nm ($n = 100$) for the calcined and 18.3 nm ($n = 100$) for the solvent extracted MCF. This again may be the result of densification at the calcination temperature of 550 °C. Figure 1g–i show TEM images of the as-synthesized MCF, the calcined MCF and the solvent extracted MCF, respectively. As shown in the Fig. 1h and the inset of Fig. 1h, the calcined MCF shows different cell structures from the as-synthesized MCF and the solvent extracted MCF, i.e., randomly organized spherical pores and onion-like cell structure called multilamellar vesicle [25], as indicated by the arrow in the inset of Fig. 1h. This heterogeneous cell structure makes pore size estimation by TEM unfeasible. On the other hand, the solvent extracted MCF shows a randomly organized cell structure similar to the as-synthesized sample.

Figure 2 shows low-angle XRD results of the as-synthesized, calcined and solvent extracted MCFs. In the case of the as-synthesized MCF, although there is a small shoulder at about 0.7°, no distinguishable peak is observed. Similarly, the solvent extracted sample shows no clear peaks,

but small shoulders at approximately 0.7° and 0.9°. The shoulders of the XRD results are broad peaks at extremely low intensities indicating a low level of pore ordering. There are two notable peaks at 0.76° and 1.10° for the calcined MCF. These 2 θ angles are equivalent to spacings of 11.63 nm and 8.06 nm, respectively. The spacings indicate the distances between orderly arranged rows of pores which include the pore sizes and the wall thicknesses. Others have also reported similar XRD peaks for the orderly arranged porous materials [26]. From the XRD results, they indicated that the calcination largely affect the arrangement of the pore structure from the synthesized stage, while the solvent extraction preserved the low-ordered pore structure.

Figure 3 shows adsorption and desorption isotherms of the as-synthesized, calcined and solvent extracted MCFs. All adsorption–desorption isotherms show type 4 hysteresis loops, indicating mesoporous structures. Analysis of the desorption isotherms of the as-synthesized MCF shows much lower pore volume compared to the other two MCFs. The adsorption branch of the solvent extracted MCF shows H2(b) type which demonstrates a complex pore networks with a large window size distribution and partially pore blocking, while the desorption branch had an additional step that resemble H5 loop. This also indicated a complex pore structure as well as partially blocked mesopores. On the other hand, the calcined MCF shows a narrower loop with parallel adsorption and desorption lines, closer to H1 type. This indicates similar distribution of window and pore sizes [27]. The difference in pore shapes and reorganized pore structure is believed to result from densification of the MCF at the high calcination temperature.

Fig. 2 XRD profiles of the as-synthesized, calcined and solvent extracted MCFs

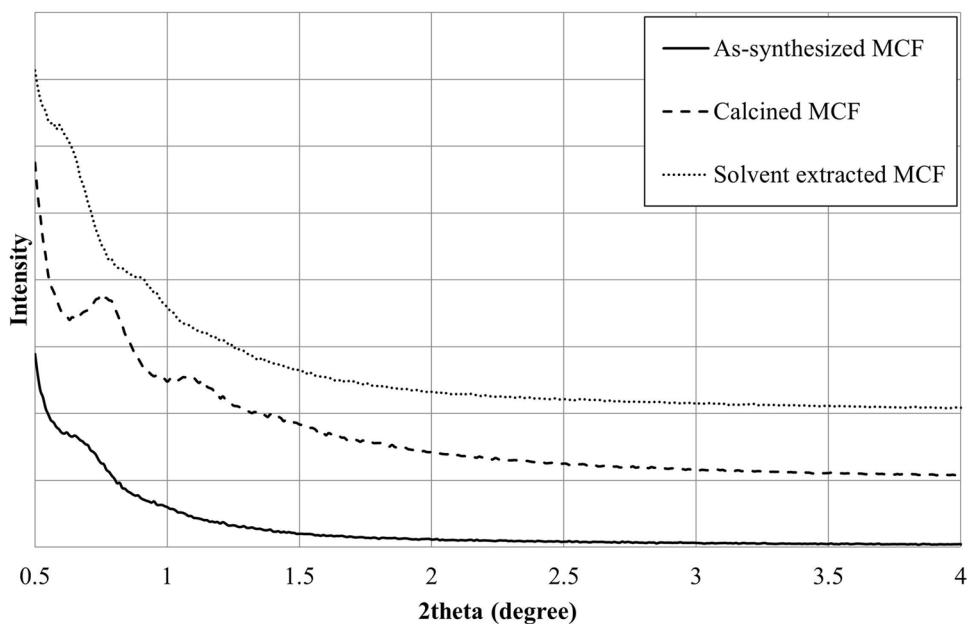


Fig. 3 Adsorption–desorption isotherms of the as-synthesized, calcined and solvent extracted MCFs

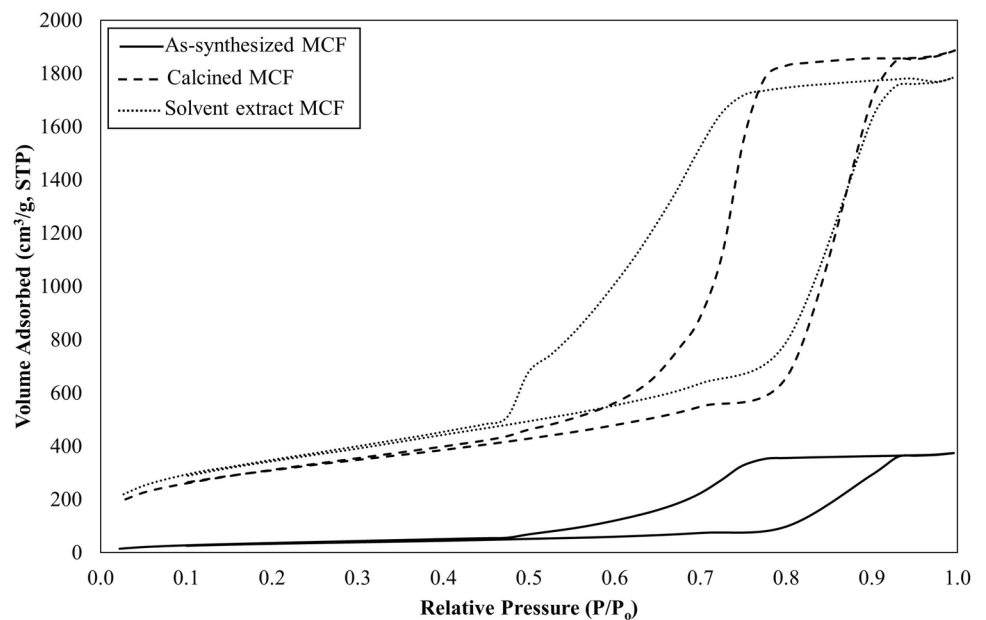


Table 1 shows surface area (BET), pore volume average pore sizes and average window sizes (Broekhoff-de Boer – Frenkel-Halsey-Hill; BdB-FHH model [24]) of the as-synthesized, calcined and solvent extracted MCFs. The BdB-FHH model is more accurate for a prediction of the ink-bottle neck pores of the MCFs. The average pore and window sizes, i.e., diameters are calculated from the adsorption and desorption branches, respectively [24]. Pore size distribution from both adsorption and desorption branches are shown in Supplementary Fig. S1. Table 1 shows that among the two template removed MCFs, the calcined sample has the larger BET surface area but the smaller average pore diameter. The average pore diameter of the calcined sample is even less than the as-synthesized MCF. This could be the result of a large scale deformation causing collapsed structure from the spherical particle, as observed in the SEM image, and a large-scale microstructural rearrangement at high temperature for the calcination, as evidenced in the XRD and SEM. In agreement with reported literature where an ordered and well-defined pore structure using this calcination temperature was also observed [7, 9, 28]. The collapsing of the mesoporous structure naturally increases the overall surface area. The high calcination temperature applied

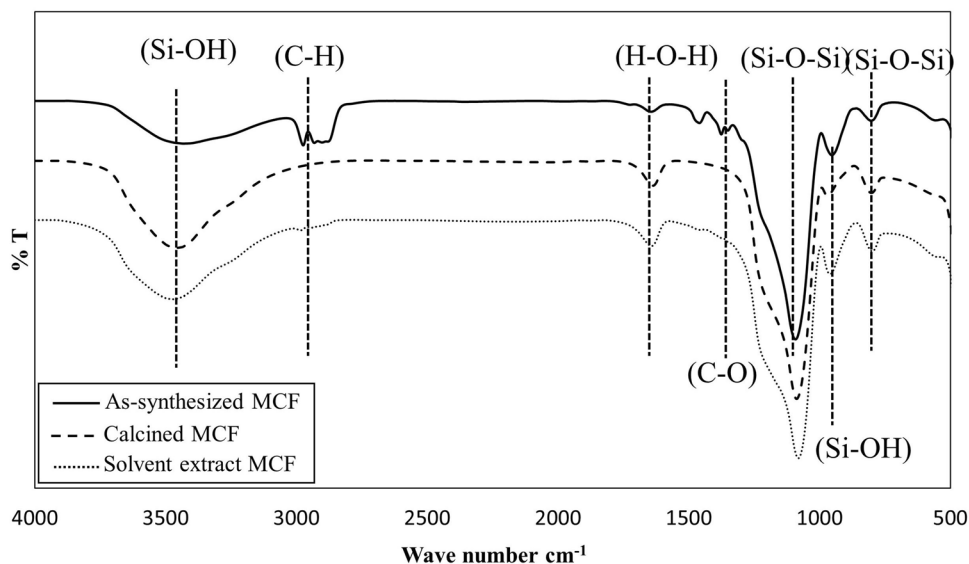
reduces pore and window sizes due to densification of the solid material. All the physical characterization results lead to a conclusion that the solvent extraction method applied for the template removal can preserve the random pore structure better than the calcination. A more complex three dimensional pore network with larger pore and window sizes than that of the calcined MCF is, hence, obtained for the solvent extracted MCF.

Fourier transform infrared (FTIR) results are shown in Fig. 4 for the MCFs before and after template removal. The FTIR adsorption spectrum of the as-synthesized MCF clearly shows C–H vibration and C–O stretching due to the existence of Pluronic P-123 respectively around 3000 cm^{-1} , and 1250 cm^{-1} , while only trace signals are detected for the solvent extracted sample. In contrast, both the C–H vibration and the C–O stretching vanish for the calcined MCF which indicates that the complete removal of chemical residues was accomplished. All MCFs clearly suggest siliceous characteristics in Si–O–Si stretching and bending vibrations at approximately 1060 cm^{-1} and 800 cm^{-1} , respectively [29]. The broad peaks at about 3400 cm^{-1} from all MCFs correspond to the stretching vibrations of internal hydroxyl group and hydrogen bonded OH groups of silica [30]. Intensities

Table 1 Surface area and pore size analysis results

	As-synthesized MCF	Calcined MCF	Solvent-extracted MCF
BET surface area (m^2/g)	125.4	1075	750
Pore volume (cm^3/g)	0.57	2.89	1.62
Average pore size (from adsorption) (nm)	11.9	10.9	18.9
Average window size (from desorption) (nm)	7.4	9.8	7.4

Fig. 4 FTIR results of as-synthesized, calcined and solvent extracted MCFs



of these broad peaks do not show significant differences between the calcined and the solvent extracted MCFs. The peaks of Si–O stretching vibration of Si–OH bulk phase at 956 cm^{-1} [31] are observed in all samples. However more pronounced intensities are noted for the as-synthesized and the solvent extracted MCFs compared to the calcined sample. This indicates more OH groups in the silica network and the incomplete condensation of the silica network in the case of the solvent extracted MCF [9].

Normalized intensities of each surface functional groups measured by ToF-SIMS are shown in the supplementary Table S1. The ratio of SiOH+/Si+ of the calcined MCF and solvent extracted MCF are 1.04 and 0.316, respectively. The ratio of OH-/O- of the calcined MCF and the solvent extracted MCF are 0.472 and 0.186, respectively. Both ratios

suggest higher amount of the surface silanol groups in the calcined MCF compared to the solvent extracted MCF [32, 33].

Figure 5 shows TGA profiles of the three MCFs. All the samples show weight losses close to $100\text{ }^{\circ}\text{C}$ due to the dehydration. Further, the as-synthesized MCF shows a large weight loss at approximately $220\text{ }^{\circ}\text{C}$ from the decomposition of the template and other chemical residuals such as the swelling agent. On the other hand, the calcined MCF shows no further weight loss after $100\text{ }^{\circ}\text{C}$ indicating complete removal of template and chemical residuals after 6 h of calcination at $550\text{ }^{\circ}\text{C}$. In the case of the solvent extracted MCF, approximately 12% of further weight loss is detected close to $400\text{ }^{\circ}\text{C}$. This temperature is slightly higher than the template decomposition temperature

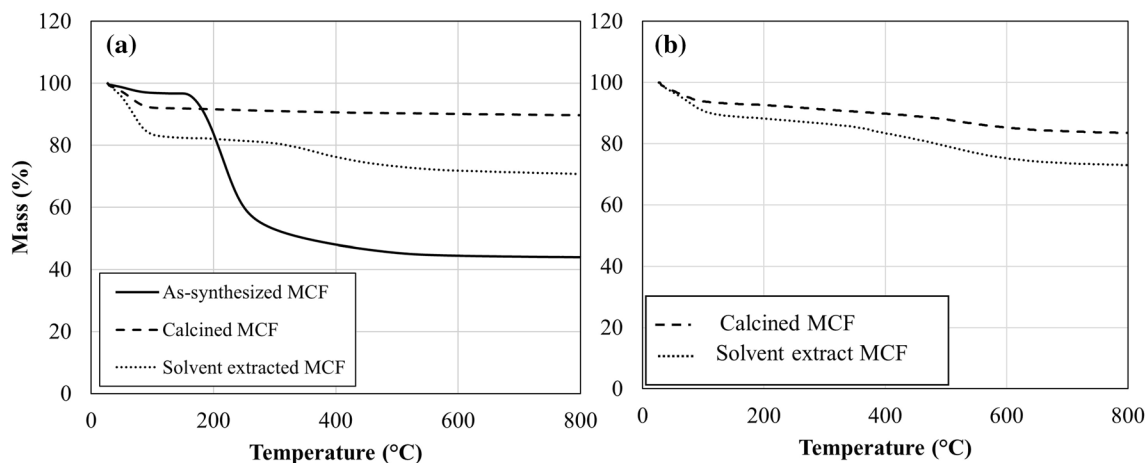


Fig. 5 **a** TGA profiles of as-synthesized, calcined and solvent extracted MCFs. **b** TGA profiles of the amine grafted calcined and solvent extracted MCFs

observed in the case of the as-synthesized MCF. It may be related to the loss of the OH groups in the MCF due to an incomplete condensation of the silica network resulting from the low temperature used for the solvent extraction process [8]. The ToF-SIMS only detects molecular species from the surface, while the TGA and FTIR collect signals from the bulk. Put together with the ToF-SIMS analysis, the results indicate that the Si–OH detected by TGA and FTIR could mainly be considered as bulk OH, or the internal Si–OH [34]. Thus, calcined MCF contained higher amounts of surface OH⁻, ready for further functionalization, compared to the solvent extract sample.

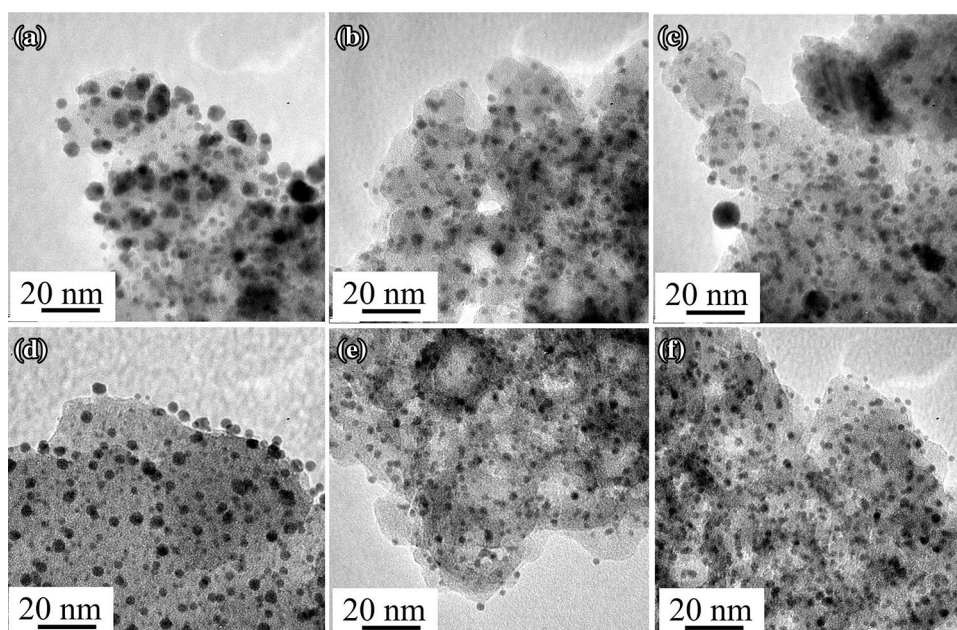
In order to decorate the MCFs with the AuNPs, the MCFs must firstly be functionalized with an amine group (APTES) before gold precursor loading to adjust the surface charges for the attachment of the negative charges (AuCl₄⁻) [35]. Figure 5b shows the TGA profiles of the calcined MCF and the solvent extracted MCF after amine grafting. After the weight loss from dehydration at approximately 100 °C, the calcined MCF loses about 8% of its weight between 300 and 700 °C, while the solvent extracted MCF loses about 15% of its weight in the same temperature range. This shows that the solvent extracted MCF is reduced by approximately 12% around 400 °C after dehydration. Accordingly, the estimated weight loss from APTES for the solvent extracted MCF was only approximately 3% while it was up to about 7.5% by weight for the calcined case. This is believed to result from the larger number of hydroxyl groups on the surface of the calcined MCF, enabling a higher amount of APTES to be grafted onto the surface. This agrees well with the ToF-SIMS results and supports the interpretation that the Si–OH found in TGA and FTIR results were mainly internal Si–OH

because the grafted APTES can only react to the surface silanol groups.

3.2 Characterization of MCFs/AuNPs and their applications as enzyme carriers

MCFs were utilized for enzyme immobilization and fabricated into enzyme biosensors. The AuNPs were objectively incorporated into the calcined and solvent extracted MCFs for the enhancement of their biocompatibility and electroconductivity. The decoration of AuNPs was achieved via an adsorption of AuCl₄⁻ to the amine terminal of APTES followed by a chemical reduction. Figure 6 shows TEM images of gold decorated MCFs with the gold precursor concentration of 10.0 mM and adsorption times of 1, 3, and 6 h, respectively, for the calcined MCF (Fig. 6a–c) and the solvent extracted MCF (Fig. 6d–f). The average sizes of the AuNPs in the calcined MCF with 1, 3 and 6 h adsorption time are 4.0 ± 1.4, 3.5 ± 1.2 and 3.1 ± 1.1 nm, respectively. While those of the solvent extracted MCFs are 3.3 ± 0.9, 2.6 ± 0.7 and 2.4 ± 0.6 nm for 1, 3 and 6 h adsorption time, respectively. It has been reported that the precursor adsorption time can affect the size and loading of the AuNPs [36]. In our case, the reduction in size of the AuNPs with longer adsorption time suggests a better diffusion of the Au precursors through the 3D pore structure of the MCF particles. Moreover, it can be clearly observed that the AuNPs decorated in/on the calcined MCF with varied adsorption times are remarkably larger than those in/on the solvent extracted MCF with a larger size distribution. This could be due to the higher density of APTES and lower diffusion rate of Au precursors in the calcined MCF resulting in a denser attachment

Fig. 6 TEM micrographs of the MCFs with 10.0 mM Au precursor adsorption time **a** 1 h, **b** 3 h and **c** 6 h for the calcined samples, and **d** 1 h, **e** 3 h and **f** 6 h for the solvent extracted samples



of Au precursors inducing coalescence crystal growth of larger AuNPs (Ostwald's ripening). Figure S2 demonstrates a cross-sectional SEM image of the calcined MCF particle after Au decoration (2 h adsorption time). The bright spots indicate the locations of the AuNPs distributed from outer surfaces and in the internal structure of the MCF. In order to evaluate the effect of the AuNPs to the electron transfer, MCFs with and without Au decoration were modified to electrodes and tested by cyclic-voltammetry using ferri-ferrocyanide as a redox couple, as shown in Fig. 7. Interestingly, incorporation of AuNPs did not help to enhance electron transfer in the case of calcined MCF, but the solvent extracted one. For the calcined MCF, potential separation between the redox peaks (ΔE_p) notably increased from 0.38 to 0.50 V, while that of the solvent extracted remarkably decreased from 0.44 to 0.27 V upon decoration of AuNPs. A more homogeneous distribution, and smaller particle size of the AuNPs in/on the solvent extracted MCF possibly resulted in effective channels for electron hopping. Thus, a much faster electrode kinetics was achieved.

Loading capacities of AChE in various MCFs and MCFs/AuNPs were next tested and the results are shown in Fig. 8. Both the calcined and solvent extracted MCFs, either pristine (denoted CB for the calcined and EB for the solvent extracted) or modified with various concentrations of AuNPs, offered similar loading capacities perhaps due to their similarities on overall physical characteristics even with pore collapsing in the cases of calcined MCFs. The windows of both MCFs were wide enough for AChE to easily pass through (AChE dimensions are $4.5 \times 6.0 \times 6.5 \text{ nm}^3$ [36]) and become entrapped in the pores. Modification

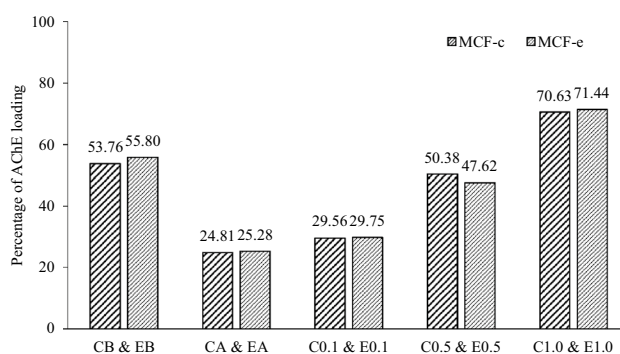


Fig. 8 Effects of MCF supports and AuNPs concentration on AChE immobilization; the calcined MCF (MCF-c) and the solvent extracted MCF (MCF-e) without surface modification (CB and EB), amine grafted (CA and EA) and concentration of gold precursor from 0.1 to 1.0 mM to % AChE loadings compared to initial enzyme amounts

of both the pristine MCFs, in contrast, caused pronounce effects on enzyme loading capacity. Comparing the unmodified MCFs, the enzyme loadings decreased dramatically after APTES grafting (denoted CA for the calcined and EA for the solvent extracted). This certainly originated from the pore blockage due to dense incorporation of APTES molecules. Interestingly, with a very small amount of decorated AuNPs (precursor concentrations up to 1 mM), AChE loadings increased tremendously. We postulate that this was due to the high sorption capacity of Au nanoparticles towards the enzyme [37, 38].

The different immobilized enzyme carriers were next fabricated into biosensors and tested for acetylthiocholine detection as a model reaction. The involved reactions are:

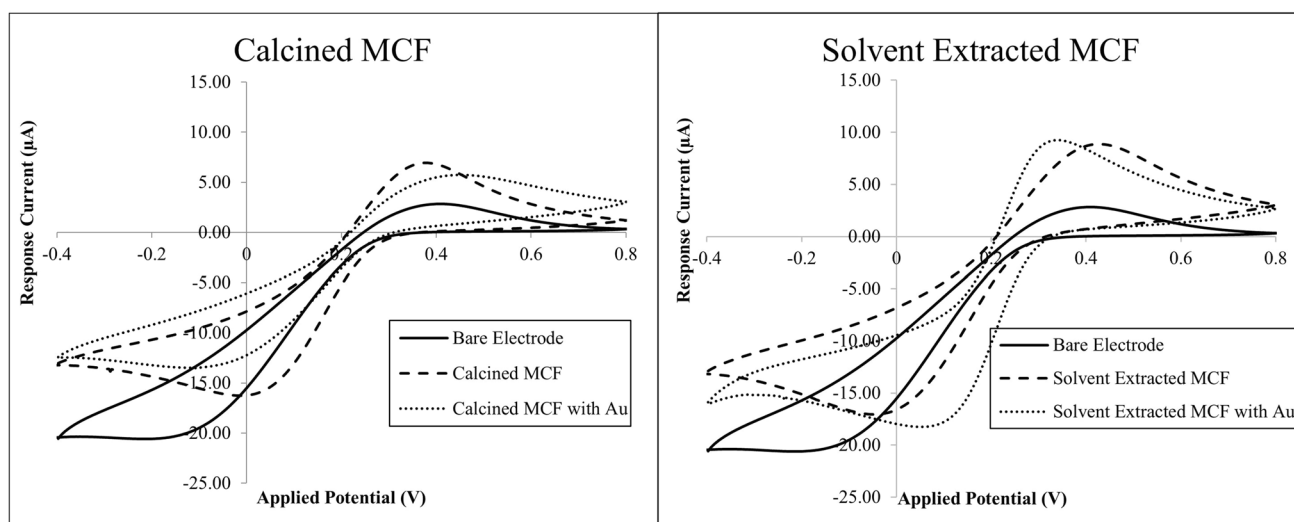
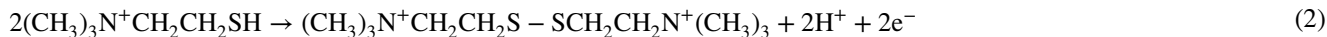


Fig. 7 CV responses were measured of modified electrodes **a** calcined MCF and **b** solvent extracted MCF with 10 mM Au precursor concentration in ferric/ferrocyanide redox couple solution (10 mM $\text{K}_3\text{Fe}(\text{CN})_6$ in 0.1 M PBS) at the scan rate of 50 mV/s



Hydrolysis of acetylthiocholine in the first reaction results in an electroactive thiocholine which then is oxidized at the electrode surface generating an oxidant current. Figure 9a, b show electrochemical responses of the biosensors based on the calcined and the solvent extracted MCFs. AChE loaded on bare electrodes showed insignificant current responses suggesting the importance of enzyme supports in distributing the enzyme molecules thus enhancing mass-transport of the associated chemicals. Higher response currents were expected for the higher enzyme loading and better electron transports in biosensors with the presence of AuNPs. However, biosensors with higher AuNPs resulted in lower peak currents both for the calcined and the solvent extracted MCFs. This indicated a mass-transfer limitation taking place. Comparing between the calcined and the solvent extracted MCFs-based biosensors, the peak currents are sharper and higher in the latter case. The lower current responses in the case of the calcined MCF could be resulted from the more condensed solid and collapse of pore structure which intensify mass transfer limitation.

Overall, even though electron microscope observations showed some collapsing of the pore structure, the calcined MCF still has a larger surface area and higher amount of silanol groups on the surface, as evidenced in the BET surface area, TGA and ToF-SIMS results. The calcined MCF

also shows a larger amount of amine grafted onto the surface than the solvent extracted MCF. These findings are based on both bulk and surface characterization techniques and are inconsistent to the works previously reported using only bulk characterization techniques [8, 39]. This emphasizes the significance of the surface sensitive characterization techniques. The properties reported in this study should have led to more AuNPs decorated on the calcined MCF surface and a higher response current when tested as enzyme biosensors in electrochemical experiments. On the contrary, the results showed that the response current of the modified electrodes with the calcined MCF was lower than those of the solvent extracted MCF. This is believed to be the effect of the collapsing of the pore structure as observed under SEM and the AuNPs sizes and distribution as observed under TEM because the size and the distribution could limit the mass transfer and result in lower response current. In this study, the template removal method was found to highly affect the surface nature of MCFs, the subsequent amine grafting, Au decorations and the current response of the MCFs modified electrodes. In optimizing the surface chemistry to give the best performance in an enzyme biosensors application, many integrated factors must be carefully studied.

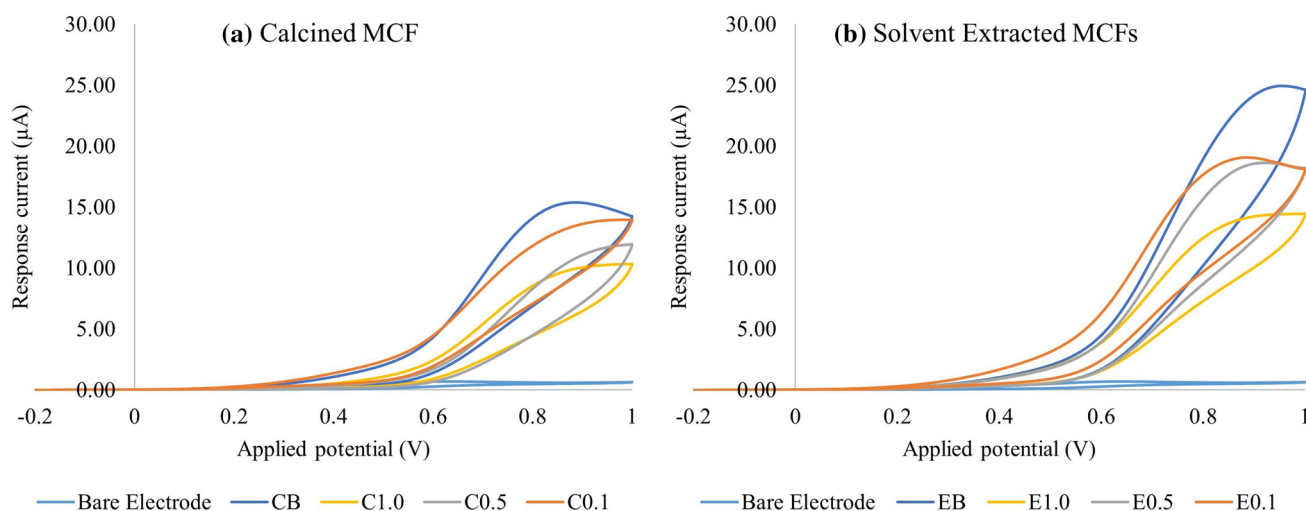


Fig. 9 Cyclic voltammograms of AChE containing AuNPs/MCF modified electrodes in phosphate buffer pH 9.0 containing 15 mM of acetylthiocholine chloride; **a** the calcined and **b** the solvent extracted

MCFs without electrode modification (Bare Electrodes), without enzyme (CB and EB) and concentration of gold precursor from 0.1 to 1.0 mM

4 Conclusion

MCFs were synthesized with two template removal methods, i.e. calcination and solvent extraction. Template removal by calcination lead to reorganization of the pores, resulting in a more orderly organized pore structure and increased BET surface area from porous structure collapse. On the other hand, the solvent extracted MCF was more microstructurally well preserved with a random 3D pore structure. Surface chemical analysis by ToF-SIMS showed that different surface functional groups remained on the MCF surface depending on the template removal method. The calcined MCF possessed more surface silanol groups; both free and hydrogen-bonded, compared to the solvent extracted MCF. The difference in the surface functional groups lead to differences in functional grafting abilities, size and distribution of AuNPs decorated on the surfaces as well as electrode kinetics. The AuNPs decorated MCFs were immobilized by enzyme AChE and modified onto electrodes for acetylthiocholine sensing. Using MCFs as supporting materials greatly improved the response currents and the electrodes modified by the solvent extracted MCF gave a better electrical response than the calcined MCFs.

Acknowledgements Authors would like to thank National Metal and Materials Technology Center (Project No. P 1550990) and Chemical Engineering Research Unit for Value Added of Bioresources and the Graduate School of Chulalongkorn University (Grant No. GCU-GR1225591009M) for financial support.

References

1. K. Holmberg, J. Colloid Interface Sci. **274**(2), 355–364 (2004)
2. A. Palmqvist, Curr. Opin. Colloid Interface Sci. **8**(2), 145–155 (2003)
3. G. Lu, X. Zhao, T. Wei, *Nanoporous Materials: Science and Engineering*, vol. 4 (Imperial College Press, London, 2004)
4. Y. Yang, L.-H. Li, Y. Li, J. Rooke, C. Sanchez, B. Su, Chem. Soc. Rev. **45**, 481–558 (2017)
5. T. Maschmeyer, F. Rey, G. Sankar, J.M. Thomas, Nature **378**, 159–162 (1995)
6. S.H. Joo, J.Y. Park, C.-K. Tsung, Y. Yamada, P. Yang, G.A. Somorjai, Nat. Mater. **8**, 126–131 (2009)
7. Y. Han, J.Y. Ying, J. Chromatogr. A **1217**, 4337–4343 (2010)
8. M. Yao, Y. Dong, X. Feng, X. Hu, A. Jia, G. Xie, G. Hu, J. Lu, M. Luo, M. Fan, Fuel **123**, 66–72 (2014)
9. C. Knofel, M. Lutecki, C. Martin, M. Martens, V. Hornebecq, P. Llewellyn, Microporous Mesoporous Mater. **128**, 26–33 (2010)
10. P. Schmidt-Winkel, W. Lukens, D. Zhao, P. Yang, B. Chemelka, G. Stucky, J. Am. Chem. Soc. **121**, 254–255 (1999)
11. Y. Han, J. Watsan, G. Stucky, A. Butler, J. Mol. Catal. B **17**, 1–8 (2002)
12. P. Schmidt-Winkel, W. Lukens, P. Yang, D. Margolese, J. Lettow, J. Ying, Chem. Mater. **12**, 686–696 (2000)
13. I. Lynch, K.A. Dawson, Nanotoday **3**(1–2), 40–47 (2008)
14. S.A. Ansari, Q. Husain, Biotechnol. Adv. **30**, 512–523 (2012)
15. M. Schumacher, M. Grun, K. Unger, Microporous Mesoporous Mater. **27**, 201–206 (1999)
16. J. Kim, S. Kim, R. Ryoo, Chem. Commun. **2**, 259–260 (1998)
17. W. Gomes, L. Cardoso, A. Gonzala, L. Aguilar, H. Andrade, Mater. Chem. Phys. **93**(1), 133–137 (2005)
18. A. Marcilla, M. Beltran, A. Gomez-Siurana, I. Martinez, D. Berenguer, Chem. Eng. Res. Des. **89**, 2330–2343 (2011)
19. P. Benjelloun, P. Van Der Voort, Cool, E. Vansant, Phys. Chem. Chem. Phys. **3**, 127–131 (2001)
20. J. Xiao, H. Li, Jin, R. Xu, Microporous Mesoporous Mater. **96**, 413–418 (2006)
21. A. Doyle, B. Hodnett, Microporous Mesoporous Mater. **58**, 255–261 (2003)
22. Y. Han, S. Lee, J. Ying, Chem. Mater. **19**, 2292–2298 (2007)
23. Z. Li, C. Kubel, V. Parvulescu, R. Richards, ACS Nano **2**(6), 1205–1212 (2008)
24. W. Lukens, P. Schmidt-Winkel, D. Zhao, J. Feng, G. Stucky, Langmuir **15**, 5403–5409 (1999)
25. N.A. Jamalluddin, A.Z. Abdullah, Appl. Catal. A **483**, 1–9 (2014)
26. D. Zhao, J. Feng, Q. Huo, N. Melosh, G. Fredrickson, B. Chmelka, G. Stucky, Science **279**(5350), 548–552 (1998)
27. M. Thommes, K. Kaneko, A.V. Neimark, J.P. Oliveier, F. Rodriguez-Reinoso, J. Rouquerol, K.S. Sing, Pure Appl. Chem. **87**(9–10), 1051–1069 (2015)
28. E.W. Ping, K. Venkatasubbaiah, T.F. Fuller, C.W. Jones, Top. Catal. **53**, 1048–1054 (2010)
29. F. Ojeda, I. Montero, F. Abel, J. Albella, Chem. Mater. **13**, 3986–3992 (2001)
30. N. Hiyoshi, K. Yogo, T. Yashima, Microporous Mesoporous Mater. **84**, 357–365 (2005)
31. X. Wang, J. Chan, Y. Tseng, S. Cheng, Microporous Mesoporous Mater. **95**, 57–65 (2006)
32. A. D'Souza, C. Pantano, J. Vac. Sci. Technol. A **15**(3), 526–531 (1997)
33. S. Takeda, M. Fukawa, Thin Solid Films **444**, 153–157 (2003)
34. L.T. Zhuravlev, Colloids Surf. A **173**, 1–38 (2000)
35. L. Gutierrez, S. Hamoudi, K. Belkacemi, Catalysts **1**(1), 97–154 (2011)
36. E. Milkani, C.R. Lambert, G. McGimpsey, Anal. Biochem. **408**(2), 212–219 (2011)
37. D. Giljohann, D. Seferos, P. Patel, J. Millstone, N. Rosi, C. Mirkin, Nano Lett. **7**(12), 3818–3821 (2007)
38. H. Qiu, C. Xu, X. Huang, Y. Ding, Y. Qu, P. Gao, Phys. Chem. C **113**(6), 2521–2525 (2009)
39. L. Wang, R.T. Yang, Phys. Chem. C **115**, 21264–21272 (2011)